Low Temperature H_2O and NO_2 Coadsorption on θ-Al_2O_3/NiAl(100) Ultrathin Films

Emrah Ozensoy, Charles H. F. Peden, and János Szanyi*

Institute for Interfacial Catalysis, Pacific Northwest National Laboratory, P.O. Box 999, MSIN K8−93, Richland, Washington 99352

Received: December 27, 2005; In Final Form: March 3, 2006

The coadsorption of H_2O and NO_2 molecules on a well-ordered, ultrathin θ-Al_2O_3/NiAl(100) film surface was studied using temperature programmed desorption (TPD), infrared reflection absorption spectroscopy (IRAS), and X-ray photoelectron spectroscopy (XPS). For H_2O and NO_2 monolayers adsorbed separately on the θ-Al_2O_3/NiAl(100) surface, adsorption energies were estimated to be 44.8 and 36.6 kJ/mol, respectively. Coadsorption systems prepared by sequential deposition of NO_2 and H_2O revealed the existence of coverage and temperature-dependent adsorption regimes where H_2O molecules and the surface NO_x species (NO_2/N_2O_4/NO_2^-,NO_3^-) form segregated and/or mixed domains. Influence of the changes in the crystallinity of solid water (amorphous vs crystalline) on the coadsorption properties of the NO_2/H_2O/θ-Al_2O_3/NiAl(100) system is also discussed.

1. Introduction

Interaction between condensed H_2O and NO_2 layers on solid surfaces has a number of significant implications for various technological and environmental applications. Treatment of NO_x emissions in automotive emissions using Pt/Rh/γ-Al_2O_3- or Pd/γ-Al_2O_3-based three-way catalysts;[1−2] NO_x abatement of diesel engine emissions via Pt/BaO/γ-Al_2O_3-based NO_x storage reduction (NSR) catalysts[3], and photochemically induced atmospheric NO_x reactions occurring on solid H_2O surfaces in the stratosphere leading to the formation of acid rain and the depletion of the ozone layer[4] can be considered as some of the important examples where interaction of NO_2 and H_2O layers plays a key role.

For this purpose, well-defined model catalyst systems serve as a convenient platform to study NO_2, H_2O, and NO_2+H_2O layers at low temperatures. A majority of the previous surface science studies on model catalysts were performed on metallic surfaces such as Au(111),[5−9] polycrystalline Au,[10] polycrystalline Cu,[11] polycrystalline Ni,[12] W(110),[13] Pt(111),[14] Pt(100),[15] Sn/Pt(111),[16] Rh(111)−Rh/Pd(111),[17] Ag(111),[18−23] and Ag(110).[24] In contrast to the metallic systems, there exists only a limited number of surface science studies focusing on the interaction of adsorbed NO_2 + H_2O layers on metal oxide surfaces in the literature.[25,26] Due to its relevance to NSR catalysts, we have previously investigated H_2O and NO_2 adsorptions on θ-Al_2O_3/NiAl(100) model catalyst support surfaces[27,28] as well as on BaO/γ-Al_2O_3 and Pt/BaO/γ-Al_2O_3 high surface area catalysts.[29−31] Our previous results indicate that H_2O adsorption on the θ-Al_2O_3/NiAl(100) surface is predominantly molecular rather than dissociative. For θ_{H2O} < 1 ML (ML = monolayer), H_2O molecules were found to populate Al^{3+} cation sites to form isolated H_2O species aligned in a row along the cation sites on the oxide surface with a repulsive interaction between them. For θ_{H2O} > 1 ML, ice multilayers were observed to form, which then desorb during temperature programmed desorption (TPD) with zero-order kinetics.[27] For the NO_2/θ-Al_2O_3/NiAl(100) adsorption system, in addition to reversible molecular NO_2 adsorption/desorption phenomena, some of the adsorbed NO_2 is converted to strongly bound nitrites and nitrates that are stable on the model catalyst surface at temperatures as high as 300 and 650 K, respectively.[28] The stability of the NO_x formed by exposing the θ-Al_2O_3 model catalyst to NO_2 increases in the order: NO_2 (physisorbed or N_2O_4) < NO_2 (chemisorbed) < NO_2^- < NO_3^-.[28] In metal-oxide or zeolite based catalytic systems, it is known that adsorbed H_2O can compete with various NO_x species on the catalyst surface by occupying/transforming available adsorption sites and, hence, result in the modification of the catalytic NO_x chemistry.[3,32,33] Therefore, in this work, we examine the NO_2 + H_2O interactions on a θ-Al_2O_3/NiAl(100) ultrathin film surface at low temperatures using TPD, infrared reflection absorption spectroscopy (IRAS), and X-ray photoelectron spectroscopy (XPS) techniques. First we will discuss the basic aspects of NO_2 and H_2O adsorptions on the θ−Al_2O_3/NiAl(100) model catalyst surface in a comparative fashion based on the results of TPD experiments. Next, the nature of the physisorbed NO_2-multilayers and their surface configuration on θ-Al_2O_3/NiAl(100) is elucidated in the presence and absence of H_2O via the IRAS technique. Finally NO_2 + H_2O coadsorption by sequential deposition of H_2O and NO_2 on θ-Al_2O_3/NiAl(100) is studied using TPD and XPS in order to investigate changes in the adsorption energies, adsorption sites, and oxidation states of the probe molecules, respectively.

2. Experimental Section

Experiments presented in this work were conducted in an ultrahigh vacuum (UHV) surface analysis chamber (P_{base} = 3 × 10^{-10} Torr) equipped with XPS, Auger electron spectroscopy (AES), a quadruple mass spectrometer (QMS) for TPD, and a rear-view low-energy electron diffraction (LEED) techniques. The main UHV chamber is coupled to a high-pressure IR cell (P_{base} ~ 2 × 10^{-9} Torr) through a set of doubly differentially pumped sliding seals, which is equipped with CaF_2 windows. The NiAl(100) single crystal used in the experiments (Princeton Scientific Corp., 10 mm diameter, 2 mm thick) was polished on both sides and spot-welded onto a U-shaped Ta wire. A C-type thermocouple was spot welded to the top edge of the crystal for temperature measurements. The NiAl(100) crystal was cleaned by alternating cycles of Ar^+ ion sputtering (V_{beam}

* Corresponding author e-mail: janos.szanyi@pnl.gov.

10.1021/jp057534c CCC: $30.25
Published on Web 03/31/2006

= 1.5 kV, I_{beam} = 1.5μA) and high-temperature UHV anneals at 1200 K. Cleanliness of the NiAl(100) sample was checked with Auger electron spectroscopy (AES) and low energy electron diffraction (LEED).

Ultrathin θ-Al_2O_3 films on clean NiAl(100) were grown by adopting a procedure that was originally suggested by Ibach and co-workers[34,35] which included saturation of the NiAl(100) surface with O_2 at 300 K (total O_2 exposure = 9000 L; 1 L = 1×10^{-6} Torr.s^{-1}) and annealing of the O-saturated surface at 1200 K in UHV for 30−60 min in order to improve the crystallanity of the oxide film.[36−38] The quality of the θ-Al_2O_3 films were checked with AES, XPS, and LEED, and typical film thicknesses were 6 Å ± 2 Å.[27]

TPD experiments were carried out using a differentially pumped QMS (UTI) by applying −70 V bias voltage on the spectrometer shield to constrain the ionizing electrons to the interior of the QMS shield to prevent any possible electron beam damage of the sample. All of the TPD data presented in this study were obtained by ramping the temperature of the crystal at a constant rate of 2 K/s. To minimize background desorption artifacts in the TPD data, a tubular pinhole doser, positioned in close proximity of the sample (∼2 mm away), was used in the adsorption experiments, which allowed the background pressure in the chamber to stay in the $\sim 10^{-10}$ Torr range during the dosing processes.

Before the introduction of NO_2 gas to the vacuum chamber, the gas dosing line and the pinhole doser were passivated by flushing NO_2 gas through the dosing lines for an extended period of time. Passivation of the dosing line was also monitored with QMS by following the 46 amu signal with respect to the 30 amu signal for a constant flux of NO_2. The saturation of the 46 amu/30 amu ratio indicated the deactivation of the surfaces used in the dosing lines. This procedure was found to be helpful to minimize the decomposition of NO_2 prior to the admittance to the vacuum chamber.

IRAS experiments were performed using a Mattson Research Series-1 FTIR spectrometer. For all of the IRAS data given here, the 1000−4000 cm^{-1} region was scanned for 16 min/spectrum (3420 scans/spec) with a resolution of 4 cm^{-1}. A background spectrum prior to each experimental series was collected from the clean θ-Al_2O_3/ NiAl(100) surface at 80 K.

XPS data were acquired with a dual anode X-ray source and multichannel electrostatic hemispherical electron energy analyzer (Omicron, EA-125), using AlKα X-rays (hν = 1486.6 eV) and a 50 eV analyzer pass energy. The X-ray source was oriented ∼50° with respect to the sample normal. XPS data were analyzed by fitting the minimum number of Gaussian peaks possible to the experimental spectra. Typical fwhm of 2.45−2.50 eV for N1s features and 2.50−2.55 eV for O1s features were used, and the resulting residual curves had a total integrated intensity of ≤3% of the corresponding experimental counterparts. Experimental XPS data were calibrated so that the Al2p metallic feature of the NiAl(100) substrate was centered at 72.6 eV. NO_2 and H_2O used in the experiments were purified by several freeze−pump−thaw cycles.

3. Results and Discussion

3.1. TPD Studies on NO_2/θ-Al_2O_3/NiAl(100) and H_2O/θ-Al_2O_3/NiAl(100). Figure 1a and b present TPD results for NO_2/ θ-Al_2O_3/NiAl(100) and H_2O/ θ-Al_2O_3/NiAl(100) adsorption systems for varying adsorbate surface coverages, respectively. A detailed interpretation of these results and the complimentary XPS data are given elsewhere.[27,28] For the NO_2/θ-Al_2O_3/NiAl-(100) adsorption system (Figure 1a), XPS,[28] and TPD experiments reveal that NO_2[39] adsorbs predominantly in a molecular fashion at low temperatures by first occupying surface cationic sites in the monolayer, resulting in a perturbed first-order desorption behavior with a temperature desorption maximum at 144 K[40] for θ_{NO2} = 1ML (ML = monolayer). After the completion of the monolayer, formation of physisorbed NO_2 multilayers is evident which leads to desorption maxima at 137 K with a typical zero-order desorption characteristics, as frequently observed for weakly bound multilayer adsorption states. The results of previous XPS studies[28] revealed that physisorbed NO_2 multilayers on θ-Al_2O_3/NiAl(100) existed in the form of NO_2-dimers (i.e., N_2O_4). Vibrational spectroscopic evidence for this assignment will be provided in the later section of the current text. Besides these molecular NO_2 states, a smaller quantity (<0.4 ML) of strongly bound NO_x surface species yielding TPD features within 180−650 K is visible as shown in the inset of Figure 1a. Based on the results of our XPS studies,[28] these features were assigned to ionic NO_x species, namely surface nitrites (NO_2^-) and nitrates (NO_3^-).

TPD data corresponding to H_2O adsorption on the θ-Al_2O_3/ NiAl(100) surface, illustrated in Figure 1b, demonstrate that, similar to NO_2 adsorption, H_2O adsorbs primarily in a molecular fashion to form, initially, a monolayer (175 K) and, subsequently, multilayers (156 K).[27] Desorption kinetics of H_2O on the θ-Al_2O_3/NiAl(100) surface shows, also very similarly to NO_2, perturbed first-order kinetics until the completion of the first monolayer, whereas the multilayer H_2O desorption takes place via zero-order kinetics as commonly observed on various solid surfaces.[41,42] H_2O desorption features appearing at $T \geq$ 250 K on oxide surfaces are commonly attributed to recombinative H_2O desorption, originating from hydroxyl groups that are formed due to the dissociation of H_2O molecules on oxide surfaces.[42] Therefore, the high temperature (250 K < T < 600 K) region of the TPD spectra given in the inset of Figure 1b implies that only about 0.10 ML of H_2O molecules dissociatively adsorb on θ-Al_2O_3/NiAl(100). Results of our vibrational spectroscopic studies also support the lack of extensive H_2O dissociation or formation of isolated hydroxyl groups on the θ-Al_2O_3/NiAl(100) surface.

The energetics of H_2O and NO_2 adsorption can be discussed in a comparative manner in the light of the data given in Figure 1a and b. It is readily seen that considering the nondissociative (or molecular) adsorption states, H_2O adsorption on θ-Al_2O_3/ NiAl(100) is stronger for both monolayer and multilayer states than that of NO_2. Since both H_2O and NO_2 molecules follow first-order desorption kinetics for $\theta_{H2O,\ NO2} \leq$ 1 ML, the Redhead approximation:[43]

$$\Delta E_{des} = RT_{max}\left[\ln\frac{\nu T_{max}}{\beta} - 3.64\right] \qquad (1)$$

where $\Delta E_{des}$is the desorption energy, R is the universal gas constant, ν is the preexponential coefficient, T_{max} is the desorption maxima for $\theta_{H2O,\ NO2}$ = 1 ML, β is the heating rate (β = 2 K·s^{-1}), can be employed to estimate ΔE_{des} values. If the values for the pre-exponential coefficients (ν) are assumed to be on the order of 10^{13} s^{-1} for both H_2O and NO_2, ΔE_{des}-$(H_2O)_{\theta=1ML}$ and $\Delta E_{des}(NO_2)_{\theta=1ML}$ can be calculated as 44.8 kJ/ mol 36.6 kJ/mol, respectively. The desorption energy values clearly show the difference in binding strength between H_2O and NO_2. It indicates that water adsorbs stronger onto the θ-Al_2O_3 surface than NO_2. Implications of this difference between the adsorption strengths will be further elaborated in Section 3.3 during the discussion of the (NO_2 + H_2O)/ θ-Al_2O_3/ NiAl(100) coadsorption system, where NO_2 and H_2O competes

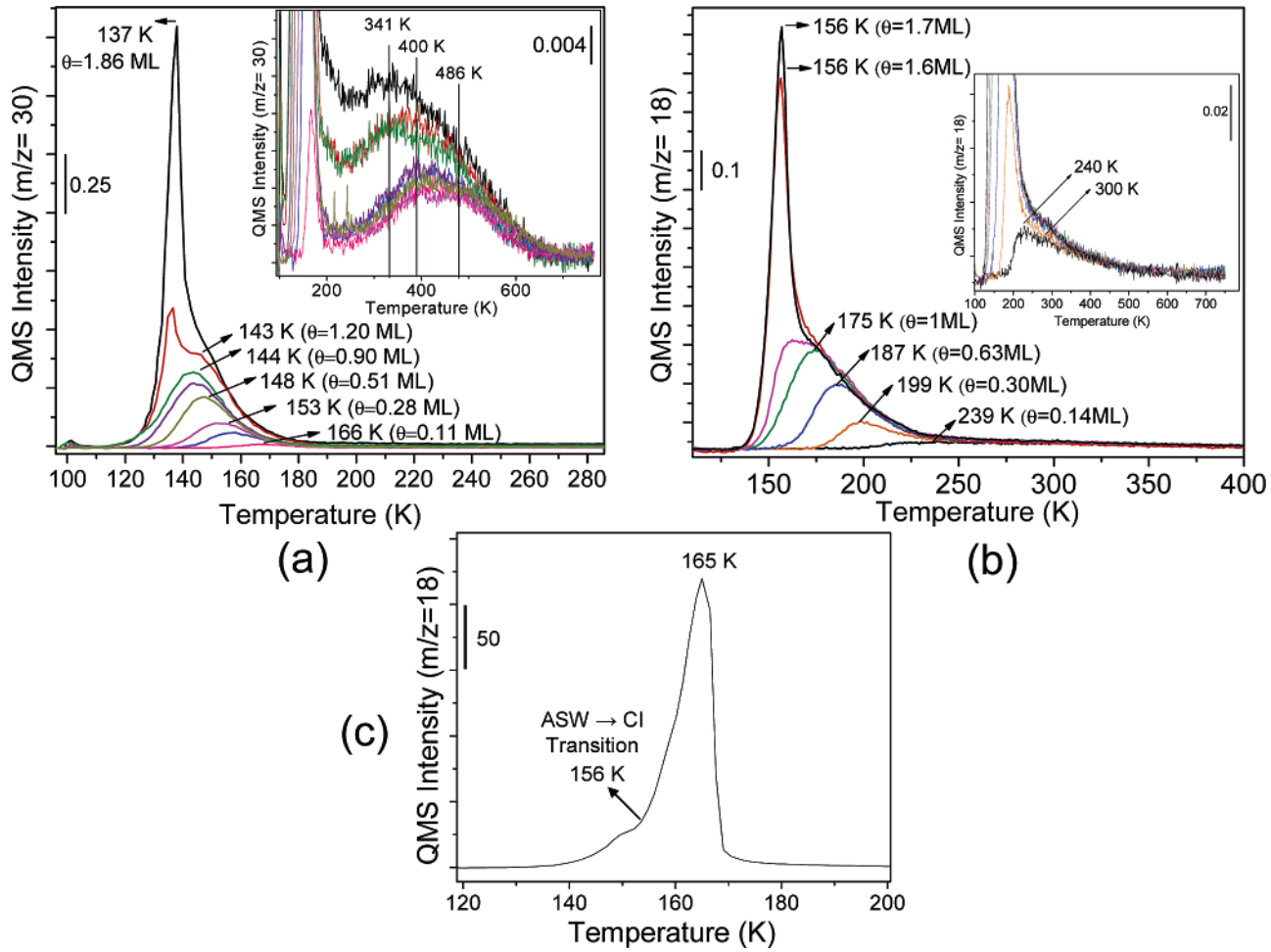

Figure 1. (a) 30 amu signal of the TPD data for various coverages of NO_2 on θ-Al_2O_3/NiAl(100). Inset gives a detailed view of the high-temperature region of the 30 amu signal. (b) 18 amu signal of the TPD data for different H_2O coverages on θ-Al_2O_3/NiAl(100). Inset gives a detailed view of the high-temperature region of the 18 amu signal. (c) TPD data for 12 ML of H_2O on $\theta-Al_2O_3$/NiAl(100). For each spectrum, adsorbates are introduced on a clean θ-Al_2O_3/NiAl(100) surface at 80 K.

for the same adsorption sites on the oxide surface. It will be shown that despite the seemingly small difference in desorption energies ($\Delta\Delta E_{des}$= 8 kJ/mol), H_2O dominates by occupying the majority of the adsorption sites of the alumina surface leading to segregated three-dimensional NO_2 domains.

TPD data presented in Figure 1c highlights an important aspect of the thermally induced changes in the crystal structure of the H_2O multilayers on solid surfaces. The TPD spectrum given in Figure 1c corresponds to a H_2O coverage of ~12 ML on the θ-Al_2O_3/NiAl(100) surface. A readily visible break point and asymmetry in the low-temperature side of the multilayer H_2O desorption feature is evident. This "pre-edge", appearing around 156 K, has also been observed during the desorption of thick (≥5 ML) H_2O multilayers from a variety of solid surfaces[41,42,44] and has been associated with a phase transition from amorphous solid water (ASW) to crystalline ice (CI). Since ASW → CI phase transition is an endothermic process, the water desorption rate in this temperature range decreases which is visible as a break point in the TPD profile. In other words, the difference between the desorption rates of ASW and CI results in the observation of a break in the TPD spectra at well-defined temperatures for given adsorbate coverages. Previous studies[7,42,45,46] suggested that for certain adsorption systems, the reactivity and the interaction of H_2O layers with other adsorbed molecules may differ depending on the crystallinity of the solid H_2O phase (i.e., ASW or CI). This point will be further elaborated in Section 3.3 during the discussion of the TPD data for the $NO_2 + H_2O$ coadsorption system on θ-Al_2O_3/NiAl(100).

3.2. IRAS Studies on NO_2/θ-Al_2O_3/NiAl(100) and NO_2/H_2O/θ-Al_2O_3/NiAl(100). Figure 2 illustrates IRAS results obtained for the low-temperature (80−146 K) NO_2 adsorption on θ-Al_2O_3/NiAl(100). The series of spectra given in Figure 2 is obtained by dosing multilayers of NO_2 on the θ-Al_2O_3/NiAl(100) surface at 80 K and, subsequently, annealing the sample to the given temperatures for a few seconds. After each annealing step, the sample was cooled back to 80 K for data acquisition. The major vibrational features observed upon NO_2 deposition appear as a very strong band at 1300 cm^{-1} and two additional strong bands at 1731 and 1760 cm^{-1}. Besides these prominent features, a low frequency shoulder at 1266 cm^{-1} and a less intense feature at 1715 cm^{-1} can be seen in Figure 2. Based on the results of previous NO_2 adsorption studies,[5−8,18,19,22,24,26] we assign the 1266 and 1300 cm^{-1} bands to the $\nu_s(NO_2)$ or NO_2 symmetric stretch of N_2O_4 monolayer and multilayers, respectively. Likewise, the bands at 1715, 1731, and 1760 cm^{-1} are assigned to the NO_2 asymmetric stretch, $\nu_a(NO_2)$, of N_2O_4 monolayer and multilayers. It should be noted that the weak feature at 1266 cm^{-1} could also be attributed to the presence of N_2O_3(a) species which may form in the reaction of background NO with the NO_2 gas. N_2O_3 adsorbed on solid surfaces results in IRAS active vibrational bands at 1265 cm^{-1} ($\nu_a(NO_2)$) and 1900 cm^{-1} (ν(NO)).[8,22] However, no bands at ~1900 cm^{-1}

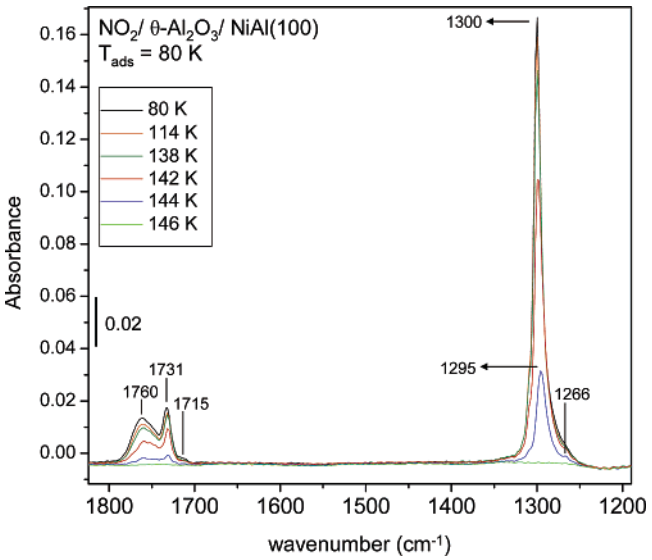

Figure 2. IRAS spectra for NO_2 multilayers on θ-Al_2O_3/NiAl(100) surface at different temperatures. Initial NO_2 exposure was made at 80 K. After the adsorbate exposure, the sample surface was annealed to the given temperatures and cooled back to 80 K for data acquisition.

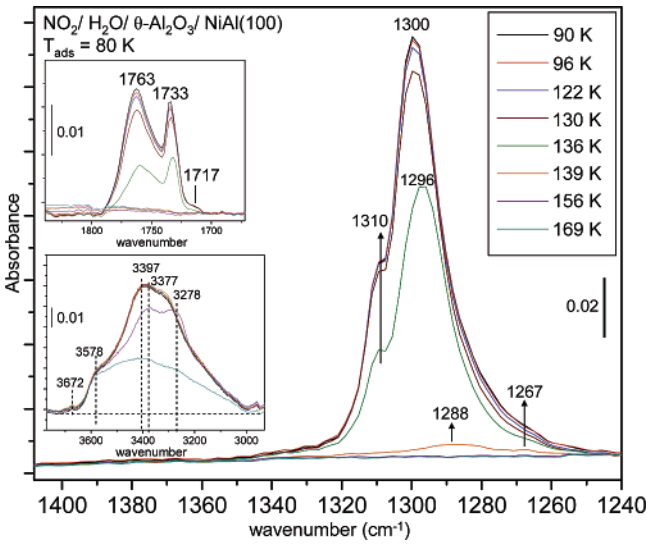

Figure 3. $\nu_s(NO_2)$ region of the IRAS spectra for NO_2 multilayers deposited on a θ-Al_2O_3/NiAl(100) surface which is initially predosed with multilayers of H_2O. Insets provide detailed views of the $\nu_a(NO_2)$ and ν(OH) regions. After the adsorbate exposures, the sample surface was annealed to the given temperatures and cooled back to 80 K for data acquisition.

were visible in our experiments, suggesting that the surface coverage of N_2O_3 is below our detection limit.

Further information regarding the orientation of the N_2O_4 multilayers on the θ-Al_2O_3/NiAl(100) surface can be deduced by comparing the relative intensities of $\nu_s(NO_2)$ (1266−1300 cm^{-1}) and $\nu_a(NO_2)$ (1715−1760 cm^{-1}) bands, taking advantage of the fact that, according to the surface selection rules for infrared radiation reflecting from a conducting solid, only the vibrational modes having a dynamic dipole moment oriented perpendicular to the surface are excited by the incident IR radiation.[47] The observed intensity ratios for the symmetric to asymmetric NO_2 stretches, $(I_{vs})/(I_{va})$, thus reveal that N_2O_4 possesses D_{2h} symmetry[5−7] where the N−N bond is perpendicular to the θ-Al_2O_3/NiAl(100) surface. This is based on the fact that the dynamic dipole moment of the $\nu_s(NO_2)$ mode of D_{2h}-N_2O_4 is directed parallel to the N−N bond while that of $\nu_a(NO_2)$ is oriented perpendicular to the N−N bond.

It should also be mentioned that the current vibrational spectroscopic results indicating the dimerization of NO_2 to form multilayer N_2O_4 layers on the θ-Al_2O_3/NiAl(100) surface at low temperatures are consistent with the results of our previous XPS experiments,[28] suggesting the presence of a nonionic N_2O_4 isomer structure. It is known from the literature[5,48−51] that N_2O_4 can also exist in the form of D-isomers, O═N−O−NO_2, which can transform into NO^+ NO_3^- (nitrosonium nitrate) at higher temperatures. The characteristic vibrational bands for D-isomers are $\nu_s(NO_2)$ at ∼1300 cm^{-1}, $\nu_a(NO_2)$ at ∼ 1640 cm^{-1}, and ν(NO) at ∼1820 cm^{-1}. Since the bands at 1640 and 1820 cm^{-1} are not observed in our IRAS results, existence of D-isomers or nitrosonium nitrate can be excluded.

In line with the TPD data presented in Figure 1a, Figure 2 shows that NO_2 multilayers in the form of N_2O_4 are weakly adsorbed on the θ-Al_2O_3/NiAl(100) surface. IRAS signal originating from the multilayers decreases with increasing surface temperatures and almost completely disappears at ca. 146 K, during which the strong $\nu_s(NO_2)$ band at 1300 cm^{-1} progressively redshifts to lower frequencies.[52]

Figure 3 illustrates IRAS results for NO_2 multilayers deposited on a thick (>10 ML) H_2O layer dosed on a clean θ-Al_2O_3/NiAl(100) substrate. Sections of the vibrational spectra relevant to $\nu_a(NO_2)$ modes (1650−1850 cm^{-1}) of NO_2/N_2O_4 and ν(OH) modes (3000−4000 cm^{-1}) of H_2O are given as insets. Similar to the NO_2 multilayers on the clean θ-Al_2O_3/NiAl(100) surface, vibrational bands at 1267, 1300 cm^{-1} associated with $\nu_s(NO_2)$ modes of N_2O_4 and bands at 1717, 1733, and 1763 cm^{-1} associated with the $\nu_a(NO_2)$ modes of N_2O_4 multilayers are also visible for $NO_2/H_2O/\theta$-Al_2O_3/NiAl(100) system. In addition to these features, a readily visible shoulder at 1310 cm^{-1} is also observed in the $\nu_s(NO_2)$ region. As this feature emerges in the presence of H_2O layers, it is most likely linked to the N_2O_4 layers that are interacting with the underlying H_2O layer resulting in a slightly different N_2O_4 orientation with respect to the isolated N_2O_4 layers. Support for a different orientation for the N_2O_4 layers interacting with the underlying H_2O layers comes from the differences in the relative intensities of the $\nu_a(NO_2)$ features at 1730 and 1760 cm^{-1} in the presence and absence of H_2O. It is apparent that the presence of H_2O leads to an increase in the intensity of the 1763 cm^{-1} band with respect to the intensity of 1733 cm^{-1} feature. IRAS data in Figure 3 also imply that, although some part of the N_2O_4 layer is interacting and, therefore, being affected by the presence of an underlying H_2O layer, isolated N_2O_4 islands still exist, whose $\nu_s(NO_2)$ bands are located at 1300 cm^{-1}. These observations are also consistent with the changes in the fwhm of the $\nu_s(NO_2)$ band in the presence and absence of H_2O (11 cm^{-1} in Figure 2 vs 17 cm^{-1} in Figure 3), suggesting that the presence of H_2O layers introduces additional adsorption sites/orientations for the N_2O_4 species resulting in a broadening of their $\nu_s(NO_2)$ bands. The spectrum corresponding to 139 K in Figure 3 suggests that as the N_2O_4 multilayer thickness decreases, $\nu_s(NO_2)$ band which was initially observed at 1300 cm^{-1} for thicker N_2O_4 layers shifts to 1288 cm^{-1} and approaches the position of the weak $\nu_s(NO_2)$ mode at 1266 cm^{-1}, indicating that the 1266 cm^{-1} feature can be attributed to NO_2/N_2O_4 molecules with a coverage close to 1 ML.

The lower inset of Figure 3 presents the section of the IRAS data where ν(OH) modes are detected. A broad and highly convoluted ν(OH) stretching band appears after the deposition of a thick H_2O layer at 80 K lies within 3300−3400 cm^{-1} and corresponds to fully coordinated H_2O molecules via hydrogen bonding in the bulk ASW network.[42] Influence of the ASW →

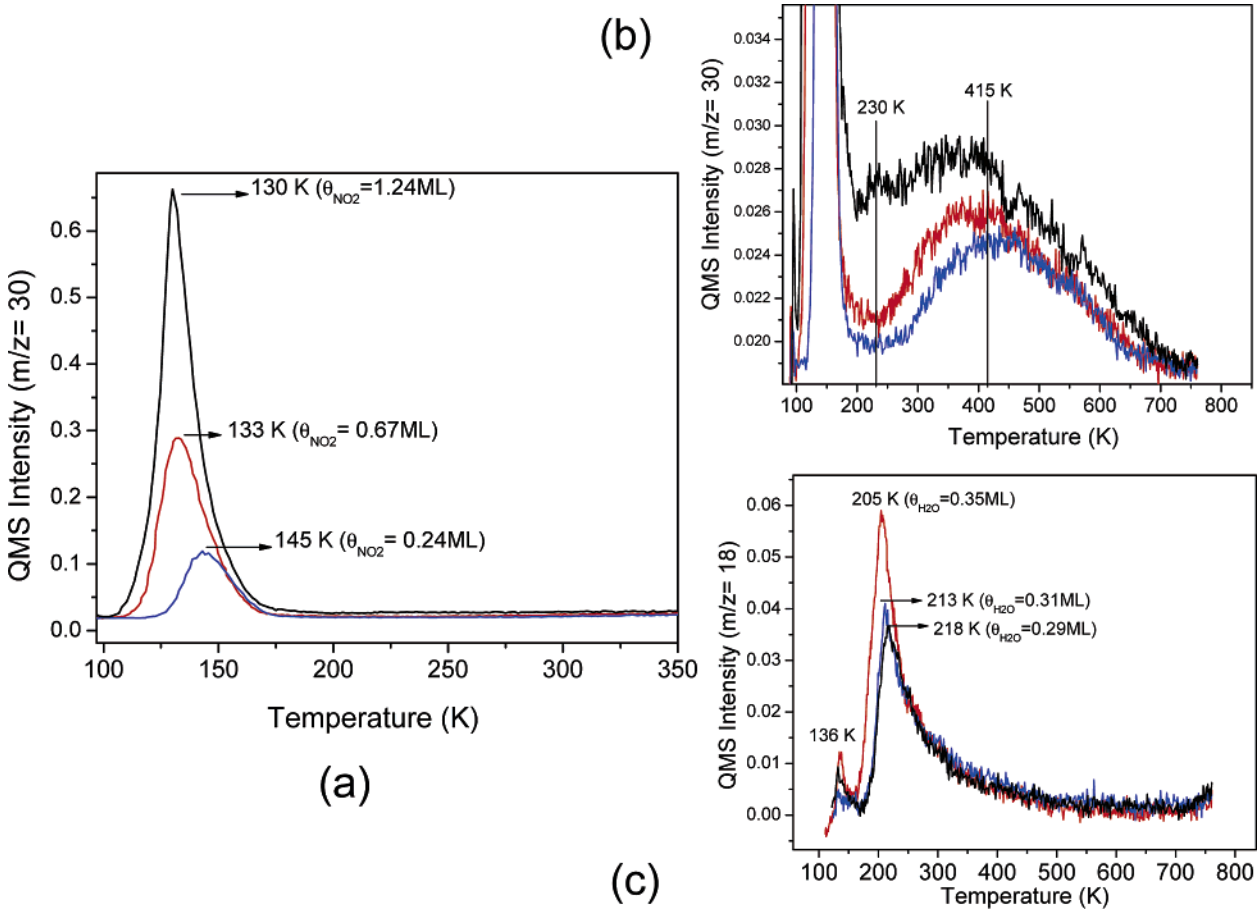

Figure 4. TPD data for NO_2 adsorption on a θ-Al_2O_3/NiAl(100) surface which is initially exposed to submonolayer (0.3 ML) coverages of H_2O. (a) 30 amu signal, (b) detailed view of the high-temperature tail of the 30 amu signal, (c) 18 amu signal. All of the adsorbate exposures were performed at a substrate temperature of 80 K.

CI phase transition on the ν(OH) modes of water layers can also be monitored in the IRA spectrum obtained at $T = 156$ K, revealing a significant ordering in the ν(OH) bands at 3300−3400 cm^{-1} and a red shift of ~20 cm^{-1}. An important aspect of the vibrational spectroscopic data given in the lower inset is the minor feature visible at 3672 cm^{-1}. In the literature[42,44] such features have been attributed to ν(OH) modes originating from uncoordinated OH bonds on the upper surface of a H_2O layer, H_2O molecules at the periphery or interior of two-dimensional water structures on solid substrates, or dangling OH bonds on the surface of 2D or 3D H_2O clusters. Data presented in the current work does not allow us to deduce a conclusive model for the exact surface morphology of the H_2O layer that is in contact with the NO_2 multilayers at 80 K on the $\theta-Al_2O_3$/NiAl-(100) substrate. Further detailed scanning probe experiments or low-temperature (<80 K) physisorption studies using weakly binding probe molecules such as N_2 or Kr would be helpful to elucidate this aspect. However, it is worth mentioning that we have not observed a significant increase in the intensity of the feature at 3672 cm^{-1} upon annealing the surface to T > 80 K, implying that the majority of the adsorbed H_2O molecules adsorb and desorb in a molecular fashion consistent with our previous TPD results.[27] From this respect, our results differ from those which suggest dissociative adsorption of H_2O on Al_2O_3/Al-(111)[53] and on Mo(110)−(1 × 6)-O[26] surfaces at T > 150 K leading to intense and well-resolved ν(OH) features at 3720 and 3584 cm^{-1}, respectively.

3.3. TPD Studies on NO_2/θ-Al_2O_3/NiAl(100) and NO_2/H_2O/θ-Al_2O_3/NiAl(100). The interaction between NO_2 and H_2O on a clean θ-Al_2O_3/NiAl(100) substrate is studied via the TPD technique by sequential deposition of these probe molecules on the sample surface using various preparation protocols. In these TPD experiments, relative coverages of each adsorbate, deposition order, and deposition temperatures were varied. A selection of the TPD results that are representative of the overall characteristics of the NO_2 + H_2O adsorption system on the θ-Al_2O_3/NiAl(100) surface is discussed below. During the TPD experiments, various possible NO_2 + H_2O reaction/desorption products such as 18 amu (H_2O), 28 amu (N_2), 30 amu (NO, NO_2, $H_xN_yO_z$), 31 amu (HNO, $H_xN_yO_z$), 32 amu (O_2), 44 amu (N_2O), 45 amu (HN_2O), 46 amu (NO_2), 47 amu (HONO), and 63 amu (HNO_3) were monitored. In the TPD experiments, the major desorption products were H_2O, NO_2, and NO. Besides these major products, smaller $H_xN_yO_z$ desorption signals were also detected similar to those that were reported on NO_2/H_2O/Au(111).[7] Intensities of these minor signals were 2 orders of magnitude or much smaller than the major desorption products which were simultaneously detected. Control experiments revealed that the quantities of these minority products were not reproducible. Therefore, they are attributed to background reactions in the QMS during the TPD experiments.

The influence of the presence of submonolayer amounts of H_2O on NO_2 adsorption was examined in the series of TPD experiments shown in Figure 4. In these experiments various amounts of NO_2 (0.2 ML < θ_{NO2} < 1.2 ML) were adsorbed on a H_2O/θ-Al_2O_3/NiAl(100) surface which was initially predosed with 0.3 ML of H_2O. In this deposition method, both of the adsorbates were introduced onto the θ-Al_2O_3/NiAl(100) surface at 80 K. As it was described in section 3.1,[28,39] the major NO_x desorption signal observed was 30 amu, which originated from

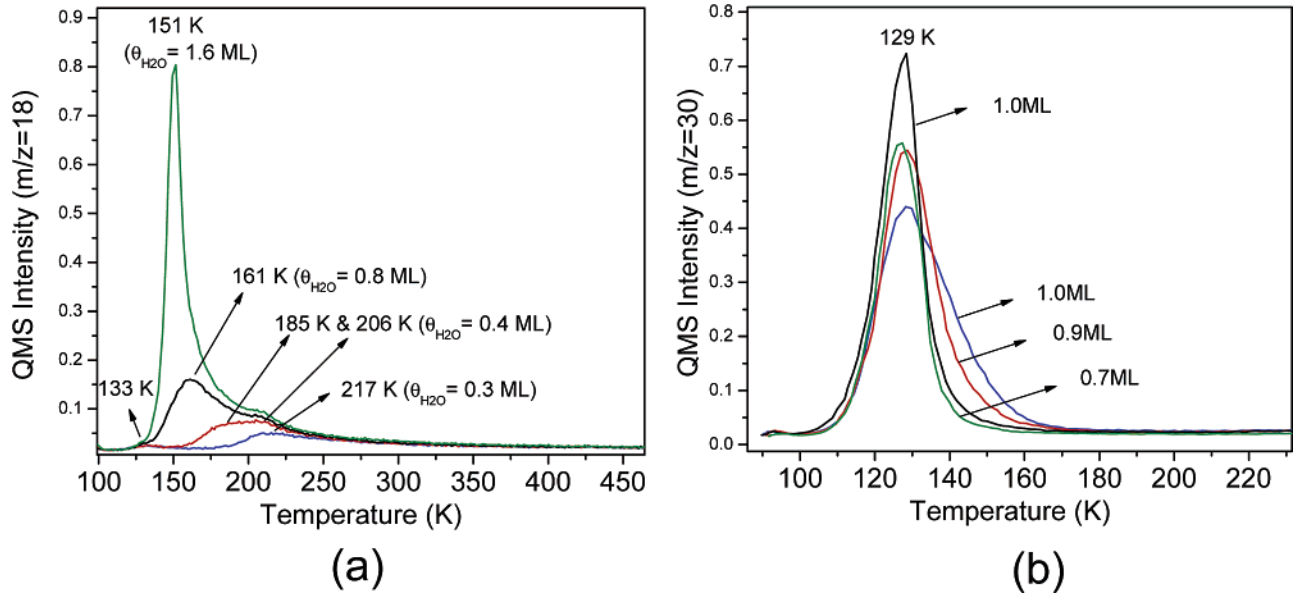

Figure 5. TPD data for various H_2O coverages (0.3−1.6 ML) on a θ-Al_2O_3/NiAl(100) surface which is initially exposed to ~1 ML of NO_2. (a) 18 amu signal. (b) 30 amu signal. All of the adsorbate exposures were performed at a surface temperature of 80 K.

NO_2 (Figure 4a) and other ionic NO_x species (Figure 4b).[28] The 18 amu signal resulting from H_2O desorption is presented in Figure 4c. Comparison of molecular NO_2 desorption features given in Figures 4a and 1a reveals that the desorption maxima in Figure 4a (corresponding to molecular NO_2 adsorption on a H_2O pre-dosed surface) shifts to slightly lower temperatures (~7 K) for the given NO_2 coverages with respect to that of Figure 1a (NO_2 adsorption on the clean substrate). Furthermore, by comparing the TPD traces corresponding to a NO_2 coverage of 1.2 ML in Figures 1a and 4a, it is evident that in the absence of H_2O, the multilayer NO_2 feature develops only after the saturation of the first layer, therefore, the monolayer and the multilayer features are easily distinguished in the TPD spectrum. On the other hand, in the presence of ~0.3 ML of H_2O, such a distinct separation between monolayer and multilayer NO_2 features is not apparent. This observation suggests that the presence of submonolayer (0.3 ML) quantities of H_2O changes the growth mode of NO_2 layers on the θ-Al_2O_3/NiAl(100) surface. On a clean θ-Al_2O_3/NiAl(100) substrate, increasing NO_2 coverage resembles a layer by layer type of growth, whereas in the presence of submonolayer quantities of H_2O, NO_2 layers grow in a form that resembles 3D clusters. These results indicate a competition for the adsorption sites between the NO_2 and H_2O molecules on θ-Al_2O_3/NiAl(100). Since H_2O binds stronger to the alumina surface than NO_2, H_2O molecules occupy the energetically more favorable adsorption sites and thus make them unavailable for NO_2 adsorption. At low NO_2 coverages, NO_2 binds to the adsorption sites on the θ-Al_2O_3 surface that are free of H_2O. However, since these sites are energetically not as favorable as those present in the absence of H_2O, the NO_2 desorption temperature shifts to lower values. At higher NO_2 coverages, the NO_2 desorption feature in Figure 4a is a composite of several origins: NO_2 directly bound to the available sites on the alumina surface, on top of weakly bound first layer NO_2, and NO_2 adsorbed on top of H_2O. The result of these multiple desorption processes is a broad, poorly resolved desorption feature. The lower temperature of the molecular NO_2 desorption maxima observed in the presence of H_2O with respect to that of the H_2O-free surface suggests the destabilization of the NO_2 multilayer by the presence of H_2O.

Figure 4b shows the formation of strongly bound NO_x species with a coverage of $\theta_{NOx} < 0.25$ ML on the H_2O(0.3 ML)/θ-Al_2O_3/NiAl(100) surface. According to the discussion above, although H_2O blocks some of the surface sites, a large number of adsorption sites remain available for NO_2 adsorption where the formation of strongly bound surface nitrates and nitrites occurs. This argument is also supported by the current XPS results to be presented in section 3.4. Water desorption signals can also be seen in more detail in Figure 4c. Comparison of Figures 1b and 4c reveals that for $\theta_{H2O} = 0.3$ ML, H_2O desorption features are shifted to higher (+15 K) temperatures in the presence of NO_x species. Since at $T > 200$ K, NO_x species existing on the surface are in the form of nitrates and nitrites,[28] the stabilization of the adsorbed H_2O molecules can be attributed to its interaction with ionic NO_x species on the surface. An additional small H_2O desorption feature at 136 K is observed in Figure 4c which is not present in Figure 1b. Figure 4a shows that this temperature is very close to the NO_2 desorption features from the H_2O(0.3 ML)/θ-Al_2O_3/NiAl(100) surface. Therefore, this feature is tentatively assigned to a small quantity of H_2O molecules that are trapped in the NO_2 matrix. It should be emphasized that despite the presence of this small portion of H_2O molecules that are trapped in the NO_2 matrix, H_2O and *molecular* NO_2 domains seem to be mostly segregated for $\theta_{H2O} \leq 0.3$ ML and $\theta_{NO2} \leq 1.2$ ML where H_2O adsorbs more strongly on the θ-Al_2O_3/NiAl(100) surface and forces NO_2 to form 2D and 3D clusters.

The coadsorption of H_2O and NO_2 on the θ-Al_2O_3 thin film was also investigated by first exposing the clean surface to NO_2 (where the NO_2 coverage is kept almost constant at ~1 ML), and then to varying amounts of H_2O (0.3 ML-1.6 ML), both at 80 K. 18 and 30 amu channels of these TPD experiments are given in Figure 5. Figure 5a shows that monolayer to multilayer transitions are observed for the H_2O layers as in Figure 1b; however, compared with the H_2O adsorption states on a clean θ-Al_2O_3/NiAl(100) surface, additional H_2O adsorption states appear, particularly for $\theta_{H2O} \geq 0.4$ ML. Examining the $\theta_{H2O} = 0.4$ ML signal given in Figure 5a reveals two poorly resolved but distinguishable desorption features at 185 and 206 K. The behavior of the lower temperature feature (185 K) resembles that observed for H_2O desorption from the clean θ-Al_2O_3 surface

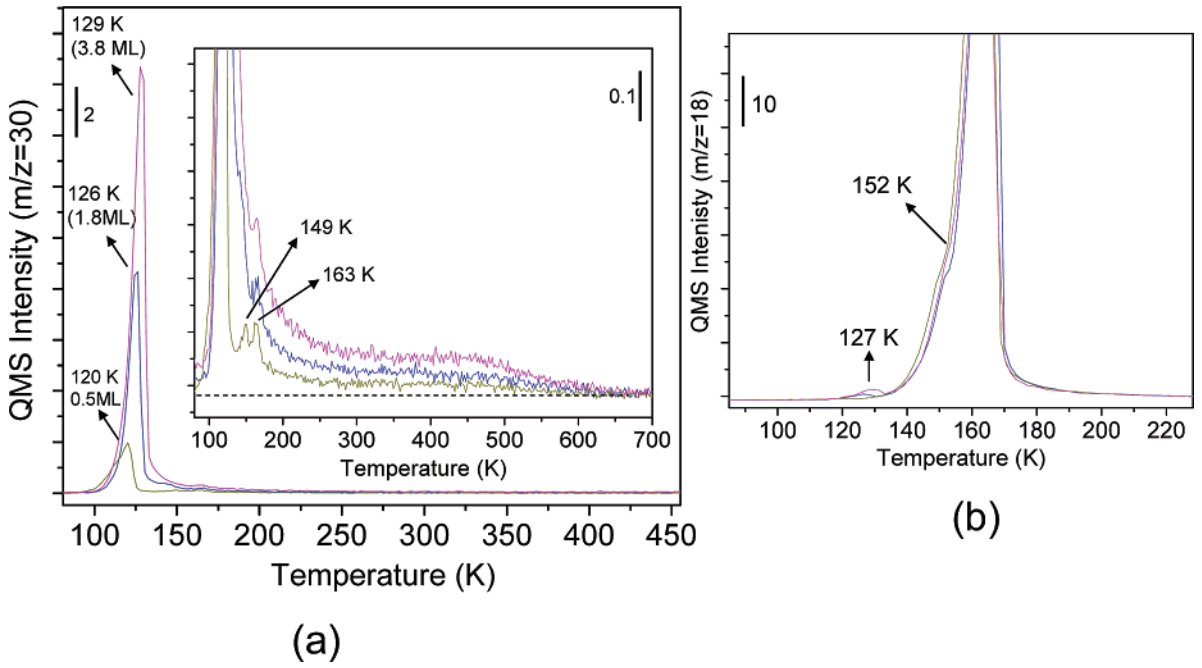

Figure 6. TPD data for NO_2 adsorption on a θ-Al_2O_3/NiAl(100) surface which is initially exposed to 10 ML of H_2O. (a) 30 amu signal where the inset depicts a detailed view of the high-temperature tail of the 30 amu signal. (b) 18 amu signal. All of the adsorbate exposures were performed at a surface temperature of 80 K.

at similar coverages (Figure 1b). The higher temperature desorption feature (206 K), however, appears at a temperature which is ~7 K higher than the one observed on the clean θ-Al_2O_3 surface. Interestingly, this high-temperature feature saturates at water coverages between 0.3 and 0.4 ML, coinciding with the coverages of ionic NO_x species (NO_2^- and NO_3^-) on the θ-Al_2O_3 surface.[28] This observation suggests that new, energetically favorable H_2O adsorption sites are created on the θ-Al_2O_3 surface after its exposure to NO_2. Therefore, these two low-temperature H_2O desorption features at 206 and 185 K can be assigned to H_2O adsorbed on alumina sites associated with the presence of ionic NO_x species, and H_2O adsorbed onto NO_x-free alumina sites, respectively. Due to its higher strength of adsorption relative to molecular NO_2 adsorption, H_2O may replace most of the adsorbed NO_2 molecules on the alumina surface, and directly interact with the alumina film. After the completion of the first H_2O layer on various adsorption sites, H_2O multilayers are formed, as evident from the desorption feature at 151 K.

There are noticeable changes in the desorption peak shape of the molecularly adsorbed NO_2 with increasing H_2O coverage, as shown in Figure 5b. At low water coverages (θ_{H2O} = 0.3−0.4 ML), NO_2, and H_2O islands directly bound to the θ-Al_2O_3 surface coexist; therefore, a high temperature shoulder (130−160 K) in the NO_2 desorption feature is present. Notably, the desorption temperature of this high-temperature NO_2 shoulder is very similar to that seen in Figure 4a when a low coverage of NO_2 was adsorbed onto ~0.3 ML of H_2O. As the water coverage increases, this higher temperature NO_2 desorption feature disappears, and at a ~1 ML H_2O dose, there is only one sharp NO_2 desorption peak at 129 K, which is located at a lower temperature than that observed for NO_2 multilayer desorption from a clean θ-Al_2O_3 surface. Note that this low-temperature feature (129 K) is the dominant NO_2 peak even at θ_{H2O} < 1 ML. Therefore, the 129 K feature is attributed to molecularly adsorbed 3D NO_2 clusters weakly bound to the H_2O adlayer modified θ-Al_2O_3 surface.

Next, we investigated the adsorption of NO_2 on a θ-Al_2O_3/NiAl(100) surface that is fully covered by H_2O molecules. For this purpose, TPD experiments were carried out by depositing NO_2 with varying coverages on a θ-Al_2O_3/NiAl(100) surface that had been dosed with ~10 ML of H_2O at 80 K prior to NO_2 exposure. The results of these experiments are illustrated in Figure 6. Figure 6a depicts the 30 amu signal originating from NO_x desorption. A detailed view of the high-temperature section of the 30 amu signal is given in the inset. Zero-order desorption behavior of NO_2 multilayers leading to temperature maxima at 120, 126, and 129 K with increasing θ_{NO2} is apparent in Figure 6a. On these water-covered θ-Al_2O_3 surfaces, regardless of the NO_2 surface coverage, NO_2 forms 3D islands as the NO_2 desorption feature resembles the TPD trace seen for multilayer NO_2 on θ-Al_2O_3. This is due to the weak interaction between NO_2 and the 10 ML-thick H_2O film.

An important aspect of the NO_2 desorption from the H_2O(10 ML)/θ-Al_2O_3/NiAl(100) surface can be seen in the inset of Figure 6a. Two sharp and distinctly resolved NO_2 desorption features are observed at 149 and 163 K. Note that the intensities of these two new desorption features are independent of the NO_2 coverage. Also, these desorption features were completely absent in TPD spectra when NO_2 desorption was studied at low H_2O coverages (<2 ML), suggesting that they are closely related to the presence of a thick H_2O multilayer on the θ-Al_2O_3 surface. Furthermore, these desorption phenomena, observed in the presence of thick H_2O overlayers occur only in a very narrow temperature window which directly overlaps with the ASW → CI phase transition. Therefore, we attribute these two distinct NO_2 desorption features to the evolution of NO_2 due to this phase transition of the H_2O layer. A number of different factors can be considered to explain the evolution of NO_2 during the crystallization of the amorphous solid H_2O layer. One of these arguments is the simple reduction in surface area or loss of porosity of the underlying H_2O layer due to the ordering of the ASW to form CI. Another possible factor is the changes in the coordination of the water molecules and the hydrogen bonding at the surface and/or inside the ice matrix during the phase

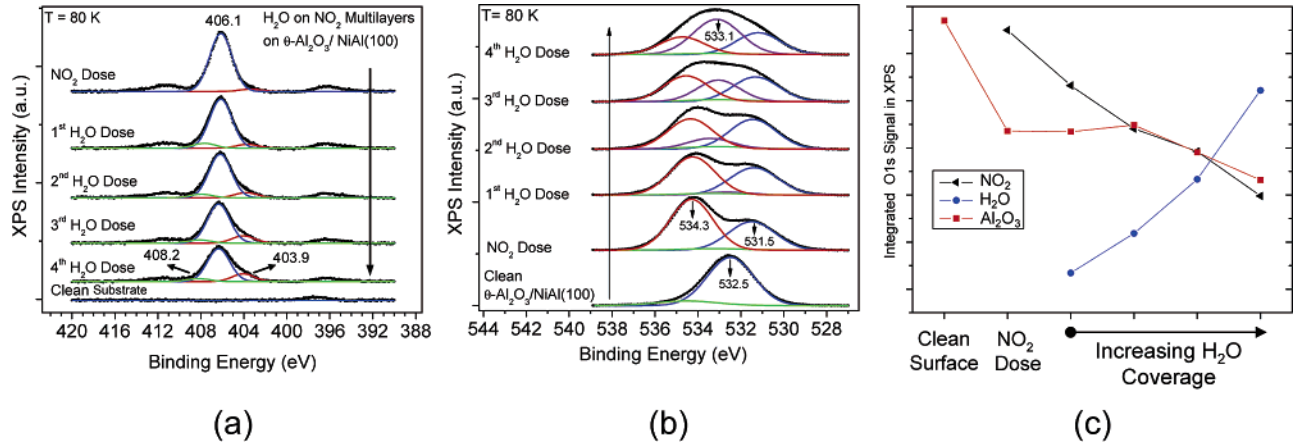

Figure 7. XPS results for successive H_2O adsorption on a θ-Al_2O_3/NiAl(100) surface which is initially covered with multilayers of NO_2 (~3 ML). (a) N1s signal. (b) O1s signal. (c) intensities of the O1s signals originating from various surface species. All of the adsorbate exposures and data acquisition were performed at 80 K. Estimated H_2O surface coverages after the given H_2O deposition steps are 0.5ML, 1.0, 2.0, and 3.0 ML.

transformation which may ultimately modify the quantity of the NO_2 molecules that can be solvated/mixed or trapped in/on the H_2O film. Some mixing of NO_2 and H_2O layers in the presence of multilayer water is also suggested by the small H_2O desorption feature at 127 K in Figure 6b. The ASW → CI phase transition can clearly be seen near 152 K during the desorption of NO_2 and H_2O from the NO_2/H_2O(10ML)/θ-Al_2O_3/NiAl(100) system. Changes in the extent of solvation or reactivity of H_2O as a function of the water crystal structure have also been previously reported. For example, using TOF−SIMS and TPD techniques, Souda[45] recently reported that the solubility of octane in amorphous solid water is much higher than that of liquid water. Along these lines, NMR and X-ray diffraction studies of Tulk, et al.[46] showed that tetrahydrofuran (THF), a water soluble cyclic ether, is forced out of the amorphous solid water solution resulting in separated THF and H_2O phases as a consequence of the ASW → CI transition. Furthermore, Wang and Koel[7] showed that for NO_2/H_2O coadsorption on a Au(111) surface, O_2 desorption is only observed in the presence of ASW but not on CI.

Another important point regarding Figure 6a is the desorption of the strongly bound NO_x species appearing within 200−650 K. As was discussed previously in our XPS study,[28] this broad desorption feature originates from ionic NO_x species, namely nitrites and nitrates. It is important to emphasize that these species are formed even in the presence of a 10 ML thick H_2O layer, which blocks a great majority (most likely all) of the available adsorption sites on the alumina surface where NO_2 can directly adsorb. Therefore, these strongly bound NO_x species observed on the H_2O(10 ML)/θ-Al_2O_3/NiAl(100) surface are either formed via solvation and diffusion of NO_2 in the ice layer and eventual adsorption on the alumina surface during the TPD experiment after the desorption of the thick H_2O multilayer, or via disproportionation reactions of NO_2 leading to nitrite and nitrate formation on the ice surface and subsequent migration of these ionic NO_x species to the alumina surface after the desorption of the H_2O multilayer.

3.4. XPS Studies on H_2O/NO_2/θ-Al_2O_3/NiAl(100). Figure 7 presents XPS results for a H_2O + NO_2 coadsorption system on θ-Al_2O_3/NiAl(100) where various coverages of H_2O (θ_{H2O} = 0.5, 1.0, 2.0, 3.5 ML, denoted as steps 1−4 in the figure) are adsorbed onto NO_2 multilayers ($\theta_{NO2} \approx$ 3 ML) at 80 K. Note that the coverage values for the XPS data are based on exposures and not additionally calibrated via TPD. N1s and O1s regions of the XP spectra are given in Figures 7a and 7b, respectively. Intensities of the O1s signals originating from different NO_x, H_2O and Al_2O_3 species are also plotted in Figure 7c for different H_2O/NO_2 doses. The topmost spectrum in Figure 7a corresponds to NO_2 multilayers deposited on a clean θ-Al_2O_3/NiAl(100) substrate. This spectrum is dominated by a N1s feature at 406.1 eV which is assigned to molecularly adsorbed NO_2/N_2O_4 species.[28] In addition to this, an additional minor feature is present at 403.9 eV which can be attributed to nitrite species.[28] As H_2O is introduced onto the NO_2/θ-Al_2O_3/NiAl(100) surface, the molecular NO_x signal starts to attenuate. This is due to the formation of 3D NO_2 clusters forming on the water overlayer. As we have discussed previously, H_2O, due to its stronger affinity for the θ-Al_2O_3 surface than NO_2, can readily diffuse through the NO_2 multilayer. As the H_2O/θ-Al_2O_3 interface develops, the NO_2 multilayer forms 3D islands on top of the H_2O layer, resulting in a decrease of the N1s signal of these NO_2 clusters with increasing H_2O coverage. H_2O deposition also leads to the development of a new N1s feature at 408.2 eV which can be assigned to nitrates. Increasing the H_2O exposure results in a slight increase in the intensity of the nitrite species, whereas the nitrate concentration remains steady (Figure 7a). Changes in the O1s region of the XP spectra can also provide additional support for the discussion above. As seen in Figure 7b, the O1s signal for the clean θ-Al_2O_3/NiAl(100) substrate is dominated by a feature at 532.5 eV. Introduction of NO_2 multilayers induces a −1.0 eV binding energy shift in the O1s features of the alumina substrate[28] and the O1s feature associated with the NO_2 layers appears at 534.3 eV. A large attenuation of the substrate O 1s feature upon the deposition of NO_2 multilayers is clearly evident in Figure 7c. Introduction of the first H_2O dose results in an intensity drop of the molecularly adsorbed NO_2 feature (534.3 eV), while that of the substrate alumina film (531.5 eV) stays almost constant. This observation indicates that the NO_2 multilayers start to form 3D clusters as soon as the first H_2O dose is introduced. This is even more evident in the XP spectrum collected after the introduction of the second H_2O dose. The intensity of the O1s of molecularly adsorbed NO_2 decreases significantly, while the peak due to adsorbed H_2O increases and the substrate feature again stays almost constant. The steady intensity of the O1s signal of the alumina substrate despite the increasing total adsorbate (H_2O+NO_2) coverage is particularly interesting. This result is consistent with an interpretation that in the early stages of the H_2O deposition, water forms a uniform layer on the θ-Al_2O_3 surface and forces the NO_2 multilayer to form large 3D clusters. Under these conditions, the photoelectron yield from the oxygen ions in alumina substrate is somewhat higher than that when a

thick NO_2 multilayer covers the θ-Al_2O_3 surface evenly. Naturally, as the water film thickness further increases (3rd and 4th H_2O dose), the XPS signal from the water layer increases significantly, eventually yielding a clearly identifiable feature at 533.1 eV, while that of the substrate decreases due to the attenuation originating from the thick water layer. The results of the XPS studies on NO_2 and H_2O multilayers on the θ-Al_2O_3/NiAl(100) surface given here are also consistent with the current TPD investigations on similar coadsorption systems (Figure 5), suggesting the formation of 3D NO_2 clusters on top of the H_2O layer in contact with θ-Al_2O_3 thin film.

4. Conclusions

In this work we examined the interaction of H_2O and NO_2 molecules on the $\theta-Al_2O_3$/NiAl(100) model catalyst surface using TPD, IRAS, and XPS techniques. Our findings can be summarized as follows:

(a) Based on the TPD experiments on H_2O/θ-Al_2O_3/NiAl(100) and NO_2/θ-Al_2O_3/NiAl(100) systems, desorption energies for H_2O and NO_2 molecules were estimated to be 44.8 kJ/mol 36.6 kJ/mol, respectively.

(b) IRAS results revealed that the NO_2 dimerizes at high surface coverages on the clean $\theta-Al_2O_3$/NiAl(100) surface and forms condensed D_{2h}-N_2O_4 (O_2N-NO_2) layers where the N−N bond is oriented parallel to the alumina surface. The presence of an underlying H_2O multilayer was found to alter orientations of some of the N_2O_4 molecules that are probably located at the H_2O/NO_2 interface.

(c) Various coverage and temperature-dependent adsorption regimes were observed in TPD experiments for NO_2/H_2O mixtures due to the competition for the adsorption sites on the $\theta-Al_2O_3$/NiAl(100) surface. In the first regime where $\theta_{H2O} < 0.3$ and 0.2 ML $< \theta_{NO2} <$ 1.2 ML, NO_2, and other NO_x species exist in mixed and segregated domains by forming 2D (N_2O_4/NO_2/NO_3^-/NO_2^-/H_2O) islands and 3D (NO_2/N_2O_4) clusters. In the second regime where $\theta_{H2O} > 0.3$ ML, H_2O molecules start to dominate the surface by occupying the majority of the available θ-Al_2O_3/NiAl(100) sites, thus forcing NO_2 molecules to form exclusively 3D clusters. At higher temperatures (such as $T > 180$ K), nitrate and nitrite species with a small surface concentration (<0.4 ML) can form mixed domains with the H_2O molecules, which leads to a slight stabilization of these adsorbed water molecules.

(d) For the NO_2 (multilayer)/H_2O(10 ML)/θ-Al_2O_3/NiAl(100) system, changes in the crystal structure of the underlying H_2O layers during the amorphous solid water → crystalline ice transition decreases the solubility/entrapment of NO_2 in the ice matrix.

(e) Strongly bound ionic NO_x species such as nitrites and nitrates are formed during TPD experiments on a H_2O/θ-Al_2O_3/NiAl(100) surface where all of the available alumina adsorption sites are blocked with 10 ML of preadsorbed H_2O molecules.

Acknowledgment. We gratefully acknowledge the U.S. Department of Energy (DOE), Office of Basic Energy Sciences, Division of Chemical Sciences for the support of this work. The research described in this paper was performed at the Environmental Molecular Sciences Laboratory (EMSL), a national scientific user facility sponsored by the DOE Office of Biological and Environmental Research and located at Pacific Northwest National Laboratory (PNNL). PNNL is operated for the U.S. DOE by Battelle Memorial Institute under contract no. DE-AC05-76RL01830. The authors acknowledge, with pleasure, Drs. Zdenek Dohnálek, Michael A. Henderson, J. Mike White, Jooho Kim, and Tykhon Zubkov for fruitful discussions.

References and Notes

(1) Heck, R. M.; Farrauto, R. J. *Catalytic Air Pollution Control: Commercial Technology;* International Thomson Publishing: New York, 1995.
(2) Ozensoy, E.; Goodman, D. W. *Phys. Chem. Chem. Phys.* **2004**, *6*, 3765.
(3) Epling, W. S.; Campbell, L. E.; Yezerets, A.; Currier, N. W.; Parks II, J. E. *Catal. Rev.* **2004**, *46*(2), 163, and references therein.
(4) Solomon S. *Rev. Geo. Phys.* **1999**, *37*(3), 275 and references therein.
(5) Sato, S.; Senga, T.; Kawasaki, M. *J. Phys. Chem. B* **1999**, *103*, 5063.
(6) Sato, S.; Yamaguchi, D.; Nakagawa, K.; Inoue, Y.; Yabushita, A.; Kawasaki, M. *Langmuir* **2000**, *16*, 9533.
(7) Wang, J.; Koel, B. E. *Surf. Sci.* **1999**, *436*, 15.
(8) Wang, J.; Koel, B. E. *J. Phys. Chem. B* **1998**, *102*, 8573.
(9) Wang, J.; Voss, M. R.; Busse, H.; Koel, B. E. *J. Phys. Chem. B* **1998**, *102*, 4693.
(10) Wickham, D. T.; Banse, B. A.; Koel, B. E. *Catal. Lett.* **1990**, *6*, 163.
(11) Rieley, H.; McMurray, D. P.; Haq, S. *J. Chem. Soc., Faraday Trans.* **1996**, *92*, 933.
(12) Brundle, C. R.; Carley, A. F.; *Faraday Discuss., Chem. Soc.* **1975**, *60*, 51.
(13) Fuggle, J. C.; Menzel, D. *Surf. Sci.* **1979**, *79*, 1.
(14) Dahlgren, D.; Hemminger, J. C. *Surf. Sci.* **1982**, *123*, L739.
(15) Schwalke, U.; Niehus, H. Comsa, G. *Surf. Sci.* **1985**, *152/153*, 596.
(16) Voss, M. R.; Zhao, H.; Koel, B. E. *Surf. Sci.* **2004**, 560, 1−3, 235.
(17) Jirsak, T.; Dvorak, J.; Rodriguez, J. A. *Surf. Sci.* **1999**, 436, 1−3, L683.
(18) Huang, W. X.; White, J. M. *Surf. Sci.* **2003**, *529*, 455.
(19) Alemozafar, A. R.; Madix, R. J. *Surf. Sci.* **2005**, 587, 1−3, 193.
(20) Polzonetti, G.; Alnot, P.; Brundle, C. R. *Surf. Sci.* **1990**, *238*, 226.
(21) Polzonetti, G.; Alnot, P.; Brundle, C. R. *Surf. Sci.* **1990**, *238*, 237.
(22) Brown, W. A.; Gardner, D. A.; King, D. A. *Surf. Sci.* **1995**, *330*, 41.
(23) Bare, S. R.; Griffiths, K.; Lennard, W. N.; Tang, H. T. *Surf. Sci.* **1995**, *342*, 185.
(24) Outka, D. A.; Madix, R. J.; Fisher, G. B.; Dimaggio, C. *Surf. Sci.* **1987**, *179*, 1.
(25) Berner, U.; Schierbaum, K.; Jones, G.; Wincott, P.; Haq, S.; Thornton, G. *Surf. Sci.* **2000**, *467*, 201.
(26) Min, B. K.; Quiller, R. G.; Deiner, L. J.; Friend, C. M. *J. Phys. Chem. B* **2005**, *109*, 20463.
(27) Ozensoy, E.; Szanyi, J.; Peden, C. H. F. *J. Phys. Chem. B* **2005**, *109*, 3431.
(28) Ozensoy, E.; Peden, C. H. F.; Szanyi, J.; *J. Phys. Chem. B* **2005**, *109*, 15977.
(29) Szanyi, J.; Kwak, J. H.; Hanson, J.; Wang, C. M.; Szailer, T.; Peden, C. H. F. *J. Phys. Chem. B* **2005**, *109*, 7339.
(30) Szanyi, J.; Kwak, J. H.; Kim, D. H.; Burton, S. D.; Peden, C. H. F. *J. Phys. Chem. B* **2005**, *109*, 27.
(31) Szanyi J. et al.; unpublished data.
(32) Wang, X. Q.; Hanson, J. C.; Szanyi, J.; Rodriguez, J. A. *J. Phys. Chem. B* **2004**, *108*, 16613.
(33) Szanyi, J.; Kwak, J. H.; Peden, C. H. F. *J. Phys. Chem. B* **2004**, *108*, 3746.
(34) Gassmann, P.; Franchy, R.; Ibach, H. *Surf. Sci.* **1994**, *319*, 95.
(35) Gassmann, P.; Franchy, R.; Ibach, H. *J. Electron Spectrosc. Relat. Phenom.* **1993**, *64/65*, 315.
(36) Fremy, N.; Maurice, V.; Marcus, P.; *J. Am. Ceram. Soc.* **2003**, *86*, 669.
(37) Fremy, N.; Maurice, V.; Marcus, P.; *Surf. Interface Anal.* **2002**, *34*, 519.
(38) Maurice, V.; Fremy, N.; Marcus. P. *Surf. Sci.* **2005**, *581*, 88.
(39) As discussed in detail in ref *28*, it is well-known that NO_2 fragments into lower mass components during its ionization in the QMS and 30 amu (NO) is dominant. Therefore, the relative intensities of the 46 and 30 amu signals, as well as the similarity between the line shapes, clearly indicate that the desorption features observed for $T < 180$ K in this work are predominantly due to the fragmentation of NO_2 in the QMS, whereas the 30 amu signal desorbing at $T > 180$ K is attributed to surface nitrates and nitrites.
(40) Temperature values given in this work are calibrated using the amorphous solid water → crystalline ice phase transition for 5 and 12 ML H_2O layers on θ-Al_2O_3/NiAl(100).
(41) Thiel, P. A.; Madey, T. E. *Surf. Sci. Rep.* **1987**, *7*, 211.
(42) Henderson, M. A. *Surf. Sci. Rep.* **2002**, *46*, 1.

(43) Redhead, P. A. *Vacuum* **1962**, *12*, 203.
(44) Daschbach, J. L.; Dohnálek, Z.; Liu, S. R.; Smith, R. S.; Kay, B. D. *J. Phys. Chem. B* **2005**, *109*, 10362.
(45) Souda, S. *J. Phys. Chem. B* **2004**, *108*, 12159.
(46) Tulk, C. A.; Ba, Y.; Klug, D. D.; McLaurin, G.; Ripmeester, J. A. *J. Chem. Phys.* **1999**, *110*, 6475.
(47) Hoffmann, F. M. *Surf. Sci. Rep.* **1983**, *3*, 107.
(48) Givan, A.; Loewenschuss, A. *J. Chem. Phys.* **1989**, *90*, 6135.
(49) Givan, A.; Loewenschuss, A. *J. Chem. Phys*. **1989**, *91*, 5126.
(50) Givan, A.; Loewenschuss, A. *J. Chem. Phys*. **1990**, *93*, 7592.
(51) Givan, A.; Loewenschuss, A. *J. Chem. Phys*. **1991**, *94*, 7562.
(52) Note that although the IRAS signal associated with the NO_2 multilayer disappears at 146 K, the surface NO_x coverage at T >146 K is not zero. This is verified by performing TPD and XPS experiments (not shown) for a NO_2 multilayer that is annealed to 150 K. The results from these experiments revealed ~0.2−0.4 ML of NO_x species desorbing during TPD within 180−600 K and the presence of surface nitrites and nitrates in N1s XPS signal with binding energy values between 403.5 and 408.0 eV. Here, we limit our vibrational spectroscopic discussion to multilayer NO_2 states. Further detailed IRAS experiments are underway to examine the nature of the NO_x species that exist after the desorption of the NO_2 multilayers on the θ-Al_2O_3/NiAl(100) surface.
(53) Chen, J. G.; Crowell, J. E.; Yates, J. T., Jr. *J. Chem. Phys*. **1986**, *84*, 5906.